Origin of Apparent Resonance Mode Splitting in Bent Long-Period Fiber Gratings

Ueyn L. Block, Vinayak Dangui, Michel J. F. Digonnet, *Member, IEEE*, and Martin M. Fejer, *Member, IEEE*

Abstract—The wavelength-selective attenuation notches generated by UV-induced long-period fiber gratings (LPFGs) have been shown to shift in wavelength and change in depth if the LPFG is bent along a curved path. Additionally, the notches frequently appear to "split" into two when the LPFG is curved. These effects have successfully allowed the realization of bend-sensing devices. Publications to date have not yielded a satisfactory physical interpretation for the apparent mode splitting. In this paper, it is shown that the spectral changes witnessed in curved LPFGs are the result of changes in the cladding-mode profiles in a bent fiber. The modes of a curved three-layer optical fiber numerically were determined and these fields are used to show that the uniform UV-induced perturbation allows coupling between the fundamental core mode and both symmetric and antisymmetric cladding modes when the fiber is curved, whereas coupling to only symmetric modes is allowed in the straight fiber. Coupling to these new modes is at the origin of new attenuation notches, which have been misinterpreted so far as mode splitting. Published devices' attenuation-notch wavelength shifts, apparent splitting, and relative depths are all well described using these changes in cladding-mode profiles.

Index Terms—Bend sensor, bent fiber, cladding mode, curved fiber, long-period fiber grating (LPFG), mode splitting, optical fiber.

I. INTRODUCTION

LONG-PERIOD fiber gratings (LPFGs) couple an incident core mode to forward-propagating cladding modes by introducing a periodic perturbation along the transmission axis of an optical fiber [1]–[3]. Introduction of the necessary periodic perturbation has been demonstrated in a variety of ways: UV illumination of a photosensitive core material [1], mechanical pressure from a corrugated plate [4], [5], and acoustically induced microbending [6], among others.

For typical single-mode optical fibers, a grating pitch of a few hundred micrometers will phase match the fundamental mode to the lowest order cladding modes at a wavelength near 1.5 μm. Incident core-mode energy is transferred to these cladding modes in the LPFG and does not recouple back into the core mode in the following unperturbed fiber. The cladding-mode energy is eventually stripped by the fiber jacket. Thus, attenuation notches are formed at the specific wavelengths where particular cladding modes are phase matched to the core mode in the LPFG.
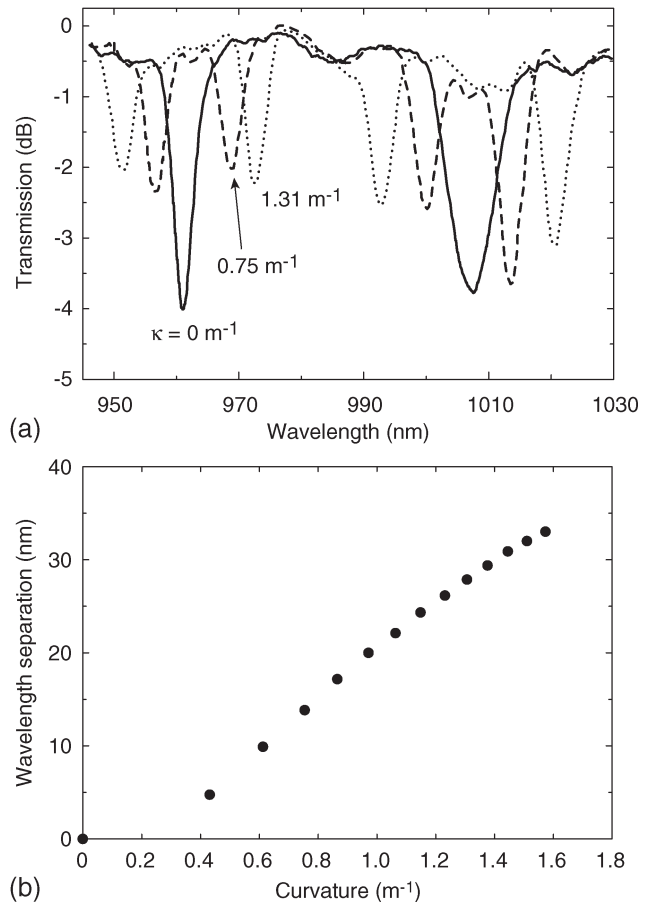
Fig. 1. (a) Transmission spectra of a 46-mm-long LPFG with a period of 600 μm and different curvatures κ. (b) Wavelength separation of notches centered near $\lambda = 1008$ nm. Data extracted from [11, Figs. 1 and 2].

The resulting wavelength-dependent filters have been used in many applications, ranging from gain flattening of optical amplifiers [7] to optical sensing of temperature, strain, and refractive index [8], [9]. Recently, the observation of spectral changes when the fiber grating is bent to follow a curved path has led to the realization of LPFG-based bend sensors [10]–[12]. Two effects are typically utilized in these devices. First, the attenuation notch present at zero curvature tends to shift in wavelength as the curvature is increased [10]. Second, notches often appear to split into two notches whose center wavelengths shift in opposing directions and depths vary with respect to each other [11]–[18].

These phenomena may be observed in the experimental results of Ye *et al.* that we have duplicated in Fig. 1 [11]. Fig. 1(a) demonstrates the emergence of new attenuation notches when
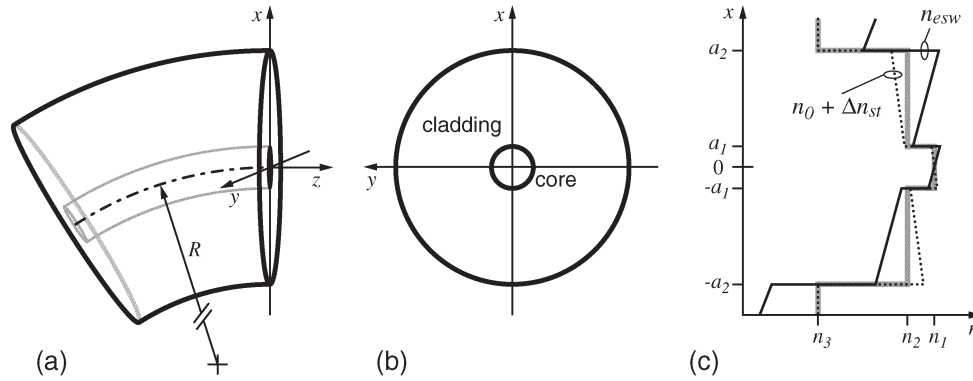
Fig. 2.   (a), (b) Geometry of curved fiber. (c) Refractive index profile ($y = 0$) of a straight fiber (solid gray line), curved fiber with longitudinal-strain-induced index change (dotted line), and effective straight waveguide (solid black line).

a UV-induced LPFG is bent, while Fig. 1(b) shows the wavelength separation of one pair of notches as the curvature is increased.

Published analyses have generally explained this apparent notch splitting by stating that the fiber curvature breaks the degeneracy of the cladding modes that are normally coupled to in the straight fiber [13], [14], [16]. These nondegenerate modes, with power concentrated on opposite sides of the fiber cladding, then propagate with different speeds due to the difference in longitudinal strain above and below the fiber axis.

We believe that this interpretation is incorrect. Since the gratings in question are UV-induced and should have a nearly uniform index change throughout the fiber core, the LPFG, when straight, can only efficiently couple to cladding modes with the same azimuthal symmetry as the fundamental LP_{01} core mode. These LP_{0n} cladding modes have a twofold degeneracy, similar to the core mode, since x- and y-polarization states have identical propagation constants. If fiber curvature were to break this degeneracy and cause the notch to split into two, then the two notches should represent orthogonally polarized cladding modes, and the device should have a large polarization dependence—in experiments, however, only weak polarization dependence has been observed [15]. Even in light of these experiments, some analyses have claimed that bend-induced birefringence, or, more specifically, the differing birefringence of core and cladding modes, is the cause of the apparent notch splitting [16], [19] even though the amount of induced birefringence at the reported levels of curvature is too small to cause such large wavelength shifts.

Additionally, if the two notches were indeed spawned from a single notch, then one would expect their separation to approach zero as the curvature κ is reduced to zero. Instead, much of the data presented in [11]–[18] show that the separation goes asymptotically to a finite nonzero value, as can be seen in Fig. 1(b), if one ignores the data point at zero curvature.

In this paper, we show that the apparent notch splitting is in fact not due to a splitting of the LP_{0n} cladding modes, but instead arises because curving the fiber:

1) changes the effective indexes of the cladding modes and of the core mode differently; and
2) breaks the cladding-mode symmetry.

Item 1) explains why the original attenuation notches, present in the straight fiber, shift in wavelength as κ is increased. Item 2) allows coupling to cladding modes with higher order azimuthal symmetry than allowed in a straight fiber, which results in new notches at nearby wavelengths. These new notches also shift in wavelength as κ is increased, although this time in the opposite direction. In [15], Chen *et al.* correctly hypothesize that the new notches are not "split" from the originals, but represent coupling to different cladding modes—but they explain this by stating that the symmetry of the UV-induced perturbation is broken, allowing coupling to different cladding modes. We demonstrate that instead, the perturbation may, and likely does, remain symmetric and that the behavior occurs because of changes in the symmetry of the modes themselves.

In addition, we predict the behavior of the notch depths as the curvature is increased and produce transmission spectra of bent UV-induced LPFGs. This analysis is achieved using numerical modeling of the modes of a curved three-layer optical fiber. This improved knowledge of the phenomena at work in a bent LPFG will aid in the development of future devices.

II. MODES OF A CURVED FIBER

The modes of a curved waveguide can be determined through the use of an equivalent straight waveguide (ESW) whose refractive index profile is modified from the bent waveguide's through a conformal transformation [20]. Marcuse [21] used this method to show that the modes of curved weakly guiding fibers tend to shift to the outer portion of the fiber as they propagate around a bend. To investigate the interaction between the core and cladding modes of a curved fiber, we must determine the modes of a three-layer cylindrical structure composed of a core, cladding, and surrounding medium.

We begin with the physical index profile of a curved fiber (Fig. 2). The bending of an initially straight fiber generates a principal strain $\epsilon_z = \kappa x$ oriented parallel to the optical axis, with $\kappa = 1/R$. Through the photoelastic effect, this strain causes an index change for both x- and y-polarization states equal to $\Delta n_{\mathrm{st}} = -(n^3/2)[(1 - \nu)p_{12} - \nu p_{11}]\kappa x$, where ν is the Poisson ratio, p_{ij} are the photoelastic constants, and n is the refractive index [22]. For a silica fiber at $\lambda = 1.55\ \mu$m, $\Delta n_{\mathrm{st}} \approx -0.31\kappa x$. The result for $\kappa > 0$ is a tilt of the refractive

index profile across the fiber cross section with a decrease in index for $x > 0$, and an increase for $x < 0$.

This physical index profile is now transformed through a conformal mapping to that of the ESW [21]. For $x \ll R$

$$n_{\text{esw}} = n(x, y)(1 + \kappa x). \tag{1}$$

Inserting the strain-adjusted index profile $n = n_0 + \Delta n_{\text{st}}$ into (1) and discarding the $(\kappa x)^2$ term results in

$$n_{\text{esw}} \approx n_0(1 + 0.69\kappa x), \qquad \text{for } r \leq a_2 \tag{2}$$

$$n_{\text{esw}} = n_0(1 + \kappa x), \qquad \text{for } r > a_2 \tag{3}$$

where n_0 is the index profile of the straight fiber and a_2 is the cladding radius. We have assumed above that the surrounding medium is air, i.e., an unjacketed fiber. Therefore, in the ESW, all three layers' indexes are modified by the curved geometry, but only the silica core and cladding experience any strain, as shown in Fig. 2(c).

This index profile was input into the Stanford Photonic Bandgap Fiber (SPBF) code, an efficient mode-solving program we originally developed for modeling photonic bandgap fibers [23]. The code uses a sparse-matrix approach to determine the modes of any waveguide index profile and has no symmetry limitations. With this program, we determined the waveguide's first 48 modes (including all degenerate states) beginning with the two polarizations of the LP$_{01}$ core mode and continuing with the first 46 cladding modes. The resulting output contains the modes' effective indexes in addition to their electric- and magnetic-field components sampled on a grid of 561^2 points extending ± 70 μm from the fiber axis in both dimensions.

We have chosen to model a step-index fiber similar to the common SMF-28 single-mode fiber with dimensions $a_1 = 4.1$ μm and $a_2 = 62.5$ μm [24]. Chromatic dispersion was modeled using the Sellmeier coefficients for SiO$_2$ and GeO$_2$ glasses [25] and assuming a pure-silica cladding around a silica core containing 0.0346 mole fraction of GeO$_2$. At $\lambda = 1.55$ μm, these parameters yield refractive indexes $n_1 = 1.44922$ and $n_2 = 1.444024$, while the surrounding medium's index $n_3 = 1.0$ (air).

The modes' symmetries were identified by viewing the field profiles. To reduce confusion, we have chosen to label modes of the entire three-layer structure with one unified nomenclature. In other words, the core mode is LP$_{01}$ and the first cladding mode with the same azimuthal symmetry is labeled LP$_{02}$ and not LP$_{01}^{\text{clad}}$, as some authors use. This convention is convenient since the labels do not change if, for instance, the wavelength is reduced below the single-mode cutoff and LP$_{11}$ transitions from being the lowest order cladding mode to a core mode. Just as they are typically defined, the first subscript numeral relates to the mode's azimuthal symmetry and the second is associated with its radial symmetry.

The dependence of the modes' effective indexes, $n_{\text{eff}} = \beta/k$, on curvature is presented in Fig. 3. The LP$_{01}$ core mode's n_{eff} has a much weaker dependence on κ than the cladding modes' since $a_1 \ll a_2$, and thus, the waveguide perturbation from the curved geometry is small in the region LP$_{01}$ occupies.
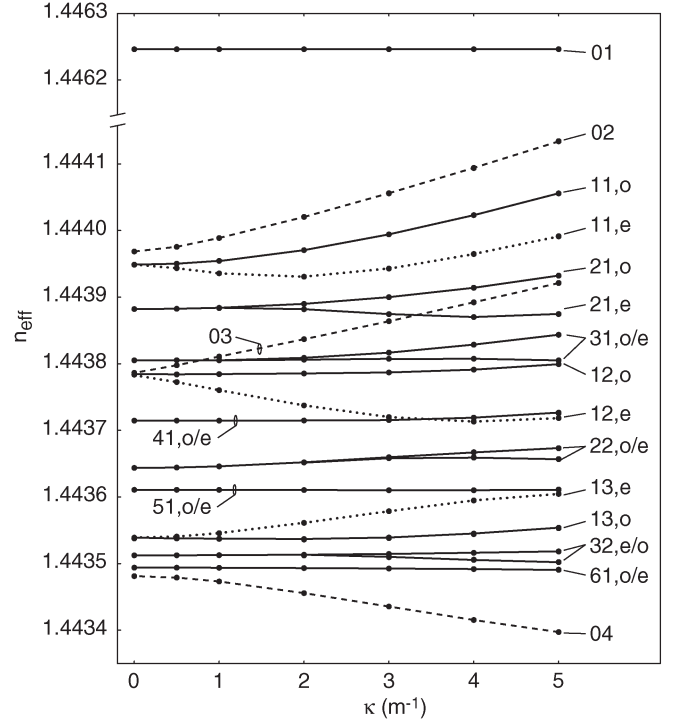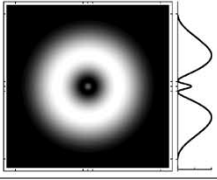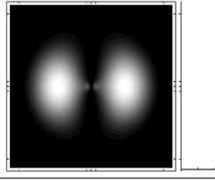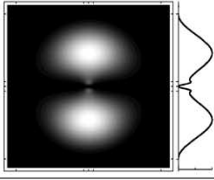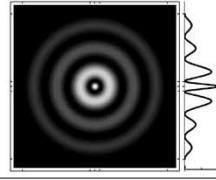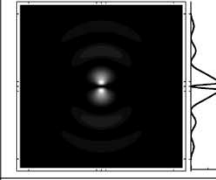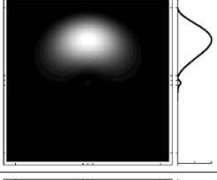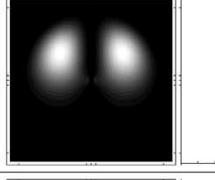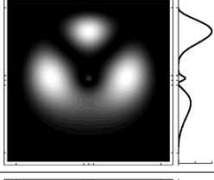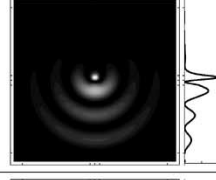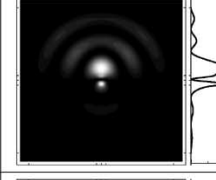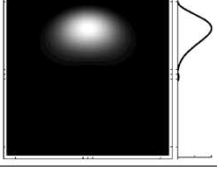

Fig. 3. Effective indexes of first 48 modes of three-layer fiber at $\lambda = 1.55$ μm. Labels indicate LP mode number and odd or even symmetry. Dashed lines indicate LP$_{0n}$ cladding modes that have nonzero overlap with the core mode—and thus form attenuation notches—in a straight LPFG. Dotted lines indicate the even LP$_{1n}$ cladding modes, which are responsible for the additional attenuation notches observed in bent LPFGs.

For most of our purposes, the core mode's index and profile can be considered constant. For other modes, the general trend is for the mode indexes to increase with κ as their power is concentrated toward the outside of the bend $x > 0$, where n_{esw} is larger. Many modes can be seen to split, though, as κ increases. These are in fact not the circularly symmetric LP$_{0n}$ cladding modes that are coupled to in a straight LPFG, but are modes with higher order azimuthal symmetry. The LP$_{1n}$ modes are the first to split, at very slight curvature. The even pair (x- and y-polarized) of LP$_{1n}$ modes, which are those with lobes oriented above and below the $x = 0$ plane, have n_{eff}'s that always tend to evolve in the direction opposite to the nearest LP$_{0n}$ mode. We will show that th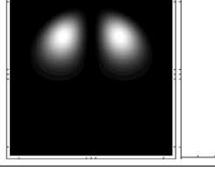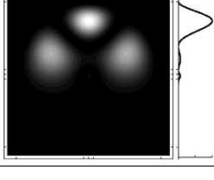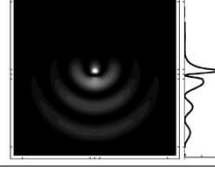ese modes, represented by dotted lines in Fig. 3, are responsible for the apparent mode-splitting behavior of curved LPFGs.

The intensity distribution of several representative modes is presented in Table I. All profiles have been normalized to the same maximum intensity. Alongside each profile is a slice of the intensity along the x-axis. Tick marks denote $x, y = 0, \pm a_1$, and $\pm a_2$ to aid in identifying the mode shape across the core of the fiber (where the UV-induced perturbation is located).

At zero curvature, the true modal description of the fiber is composed of hybrid-electric, transverse-electric, and transverse-magnetic modes (HE/EH, TE, and TM), each of which have circularly symmetric intensity profiles. As curvature is introduced, the asymmetry causes the modal basis to be composed of modes that are strongly linearly polarized with multiple azimuthal lobes. The SBPF code therefore outputs the non-LP modes when $\kappa = 0$. In order to more clearly

TABLE I
INTENSITY PROFILES OF SELECTED MODES AT $\lambda = 1.55$ μm FOR DIFFERENT FIBER CURVATURES κ

demonstrate the mode evolution as κ is increased, the $\kappa = 0$ modes shown in Table I have been filtered through a virtual linear polarizer. The nondegeneracy of the actual modes comprising these approximately LP modes is negligible for the purposes of this discussion.

The profiles for $\kappa = 0$ (see Table I) clearly show why coupling occurs between the core mode and LP_{0n} cladding modes in a UV-induced LPFG that remains straight. These modes have a local maximum in the intensity at the fiber center and are symmetric about that point, similar to the core mode. As κ is increased, the power in the LP_{02} mode tends to shift toward the outside of the bend ($x > 0$), just as water would if traveling around a bend in a pipe. This shift is accompanied by a reduction in the relative power residing within the core of the fiber as the original local maximum now shifts toward $x < 0$ and shrinks in size. A similar evolution is present with LP_{03} (not shown). For the LP_{04} mode, the exact opposite profile shift occurs: power concentrates more toward $x < 0$, and again, the central peak shifts away from the fiber center (toward $x > 0$). As expected physically, the overall shift of power toward positive or negative x correlates well with the changes in n_{eff} seen in Fig. 3. We do not have a qualitative explanation for why some modes concentrate toward $x < 0$, where the ESW index is reduced, except to state that this set of modes satisfy the orthogonality condition.

Likewise, because of the symmetry of UV-induced LPFGs, it is obvious that LP_{1n} modes do not ordinarily couple with the core mode. Their profile, for both odd and even lobe arrangements, is always antisymmetric across the fiber center. This results in the zero intensity seen at $x = y = 0$ (see Table I). The lobes on either side have opposite phase, and thus, the overlap with the core mode and symmetric UV-induced perturbation is zero.

The odd LP_{1n} modes, whose fields are antisymmetric across the x-axis, continue to have zero overlap with the core mode

as they shift toward $x > 0$ with increasing κ. The even LP_{1n} modes, however, undergo more drastic changes (see Table I). The curvature again causes the modes' lobes to shift along x, but this shift now causes some power to begin to resonate within the core region. The field profile is no longer antisymmetric across the fiber core. This effect now allows the even LP_{1n} modes to couple with the LP_{01} core mode when a UV-induced LPFG is bent.

III. WAVELENGTH SHIFTS IN BENT LPFGS

In an LPFG, attenuation notches appear at wavelengths λ_m where the core mode and a particular cladding mode m satisfy the phase-matching condition

$$\lambda_m = \left(n_{\text{eff}}^{\text{co}} - n_{\text{eff}}^{\text{cl},m} \right) \Lambda = \Delta n_{\text{eff}}^m \Lambda \qquad (4)$$

where Λ is the grating period. Δn_{eff}^m is wavelength dependent; its form is critical in determining the exact notch location.

Using our numerical method to determine the bent fiber modes at a large number of wavelengths is a cumbersome task. For this reason, we have chosen to run the simulation at discrete wavelengths separated by 50 nm and linearly interpolate the results to determine the modes' propagation constants at all wavelengths between 1.2–1.6 μm. These simulations were carried out for the same fiber parameters as given earlier. The resulting phase-matched wavelengths versus fiber curvature are shown in Fig. 4 for a grating with a period $\Lambda = 560$ μm.

The phase-matched wavelengths corresponding to the first three symmetric cladding modes LP_{02}–LP_{04} can be seen in Fig. 4 to shift by up to 45 nm as the fiber curvature is increased from 0 to 5.0 m^{-1}. Likewise, the phase-matched wavelengths for $LP_{11,e}$, $LP_{12,e}$, and $LP_{13,e}$ at zero curvature are very similar to those for LP_{02}, LP_{03}, and LP_{04}, respectively. Each
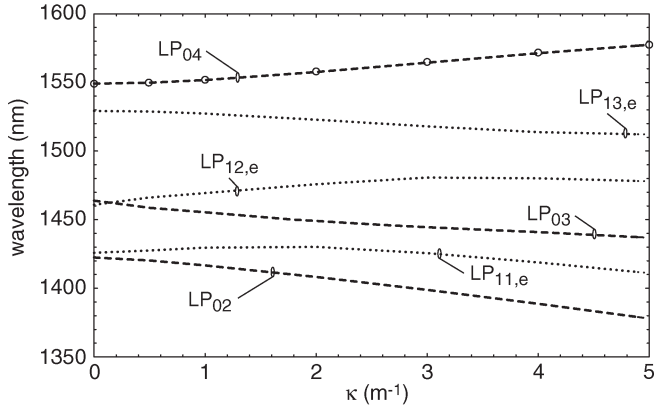
Fig. 4. Center wavelengths of attenuation notches $\Lambda = 560$ μm. Curves were generated using data interpolated between discrete simulated wavelengths $\lambda = 1200, 1250, \ldots, 1600$ μm. Dashed curves indicate LP_{0n} cladding modes that form attenuation notches in a straight LPFG. Dotted curves indicate the even LP_{1n} cladding modes, which are responsible for the additional attenuation notches observed in bent LPFGs. Circles are LP_{04} notch wavelengths estimated using only the simulation at 1550 nm, as discussed in (5).

Fig. 5. Relative coupling strength of first three LP_{0n} and LP_{1n} cladding modes versus fiber curvature at $\lambda = 1.55$ μm.

of these antisymmetric modes shifts in the opposite direction compared to its LP_{0n} counterpart. The existence of nonzero mode overlap between the core mode and these antisymmetric cladding modes when $\kappa > 0$ will generate the appearance of mode-splitting behavior as attenuation notches are formed at the phase-matched wavelengths shown in Fig. 4.

One can estimate the magnitude of a notch's wavelength shift by using data collected at a single wavelength. This simplification is useful because the collection and analysis of simulation data can be quite time consuming. We demonstrate this using our simulation results at $\lambda = 1.55$ μm (Fig. 3) and estimate the shift of the LP_{04} notch, which is located near this wavelength at zero curvature due to our choice of grating period. We start by using an analytic solution of Maxwell's equations in a straight three-layer fiber [26] to determine $n_{\text{eff}}(\lambda)$ for LP_{01} and LP_{04} and thus $\Delta n_{\text{eff}}^{LP_{04}}(\lambda)$. Since without numerical simulation we have no information regarding the wavelength dependence of n_{eff} for a bent fiber, we shall assume it is the same as when $\kappa = 0$. In other words, the addition of curvature simply increases or decreases $\Delta n_{\text{eff}}^m(\lambda)$ uniformly in the vicinity of $\lambda = 1.55$ μm by the amounts shown in Fig. 3. This approximation is valid because the wavelength dependence of $\Delta n_{\text{eff}}^m|_{\kappa=0}$ is dominated by the waveguide dispersion of n_{eff}^{co} and, as we have already shown, the core mode's effective index is quite insensitive to bending.

Easily derived from (4), the change in notch central wavelength with respect to a change in Δn_{eff}^m is

$$\frac{d\lambda_m}{d\left(\Delta n_{\text{eff}}^m\right)} = \left[\frac{1}{\Lambda} - \frac{d\left(\Delta n_{\text{eff}}^m\right)}{d\lambda}\right]^{-1} \quad (5)$$

to first order. Using $\Lambda = 560$ μm and $\Delta n_{\text{eff}}^{LP_{04}}(\lambda)$ for a straight fiber, we find that $d\lambda_m/d(\Delta n_{\text{eff}}^{LP_{04}}) = 3.23 \times 10^{-4}$ m. This value, when multiplied by the numerically obtained bending-induced changes in mode index from Fig. 3, results in a good estimate of the notch wavelength shift (see Fig. 4).
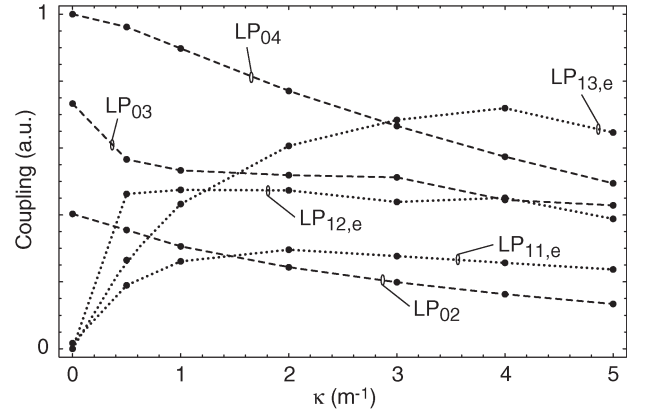
IV. COUPLING STRENGTH

The amount of energy coupled from the core mode to a cladding mode in an LPFG is dependent upon the overlap of the two modes and the induced waveguide perturbation [3]. Ideally, the UV-induced perturbation is uniform across the fiber core and zero elsewhere, and thus, the coupling constant is proportional to the overlap integral

$$I_m = \int_0^{2\pi} \int_0^{a_1} \mathbf{E}_{\text{co}}^{\text{t}} \cdot \mathbf{E}_{\text{cl},m}^{\text{t}*} r\,dr\,d\phi. \quad (6)$$

We compare the relative coupling strength versus curvature for several cladding modes by numerically evaluating the above integral. The modes' transverse electric fields $\mathbf{E}^{\text{t}}$ have been normalized such that each mode carries the same power. The results of this numerical integration at $\lambda = 1.55$ μm are presented in Fig. 5.

At $\kappa = 0$, the LP_{1n} cladding modes have zero coupling due to their antisymmetric profile. The slight departure from this behavior seen in Fig. 5 is attributed to numerical error. As κ is increased, the coupling to these modes rises rapidly before beginning to decrease at larger κ. In contrast, the level of coupling to LP_{0n} modes tends to monotonically decrease across the calculated range of curvatures. These results agree well with the qualitative description presented above and with published experimental observations [11]–[18], including Fig. 1.

Some experimental results show that for some cladding modes, the wavelength "splitting" $\Delta\lambda$ goes to a finite, nonzero value as $\kappa \to 0$ [11], [12], [17], [18]. For example, the data in Fig. 1(b) do not appear to approach 0 as $\kappa \to 0$ if one excludes the value at the origin. This correlates well with Fig. 5, namely as $\kappa \to 0$, coupling of the LP_{1n} cladding modes goes to zero, and we do not see the notches anymore since they have zero depth. This is likely the reason why it was assumed that the notches originated from the same notch as that which already exists at $\kappa = 0$, and the datapoint at the origin was included in Fig. 1(b).

Nonzero coupling strengths also occur for higher azimuthal-order cladding modes that have the proper lobe arrangement ($LP_{2n,e}$, $LP_{3n,e}$, etc.). These cladding modes should also

generate new LPFG attenuation notches not present in the straight LPFG. Ever-larger curvatures are required to increase the coupling a given amount from zero for each increasing azimuthal order, thus making these notches sizable enough to be noticeable. For instance, within the range $0 < \kappa < 3$ m^{-1}, none of the above modes would exceed 25% of the coupling strength of LP$_{04}$ at zero curvature. Since the resulting attenuation notches are secondary to those presented above, we do not present any analysis of these modes.

V. TRANSMISSION SPECTRUM OF BENT LPFG

The above analysis was repeated for $\lambda = 1.2, 1.25, \ldots,$ 1.6 μm, and the resulting mode overlaps were linearly interpolated to span the entire wavelength band and $0 < \kappa < 5$ m^{-1}. The transmission spectra of bent LPFGs were then calculated using the interpolated effective index and these overlap values. The coupled-mode equations [3] were numerically integrated along the length of a 25-mm-long grating every 0.5 nm across $\lambda = 1375 - 1600$ nm. The coupled-mode equations were derived assuming a sinusoidal perturbation with a square envelope. Additionally, the self-coupling terms were neglected. This assumption essentially implies that the periodic UV-induced index change had no dc component. The presence of a dc perturbation component and self-coupling terms would add an overall wavelength shift to the transmission spectra but would not affect the bend-induced behaviors we are studying. The grating period $\Lambda = 560$ μm and amplitude of the coupling coefficients were chosen such that a 6-dB notch is present at $\lambda = 1550$ nm in the straight fiber. At each wavelength, the amount of core-mode power remaining at $z = 25$ mm was used to assemble a transmission spectrum. Spectra for $\kappa = 0 - 3$ m^{-1} are shown in Fig. 6.

The first attenuation notch seen in Fig. 6(a) at $\lambda \approx 1425$ nm is generated when the core mode couples to the LP$_{02}$ cladding mode in an unbent fiber. As the curvature is increased, this notch moves toward smaller λ and shrinks in size. Simultaneously, a new notch is formed by coupling with LP$_{11,e}$ and shifts toward larger λ while initially growing in size before it eventually begins to shrink. A similar behavior is observed for the second notch of the unbent fiber at $\lambda \approx 1460$ nm, which corresponds to LP$_{03}$. One notable difference is that the LP$_{12,e}$ notch, which appears near the LP$_{03}$ notch when bending is introduced, reaches its maximum depth very quickly and then proceeds to shrink as it migrates toward longer λ.

Near $\lambda = 1550$ nm, the relative wavelength shifts are reversed. The initial LP$_{04}$ notch's depth decreases while it moves toward larger λ with increasing curvature. When curvature is introduced, a notch corresponding to LP$_{13,e}$ appears, which continues to increase in size and shift in the opposite direction. As seen in Fig. 6, the general behavior of the initial attenuation notches and those that appear only after curvature is introduced follows the expected trends discussed in Sections III and IV.

VI. DISCUSSION AND CONCLUSION

As presented above, the introduction of curvature κ has three primary effects on an LPFG. First, the center wavelengths

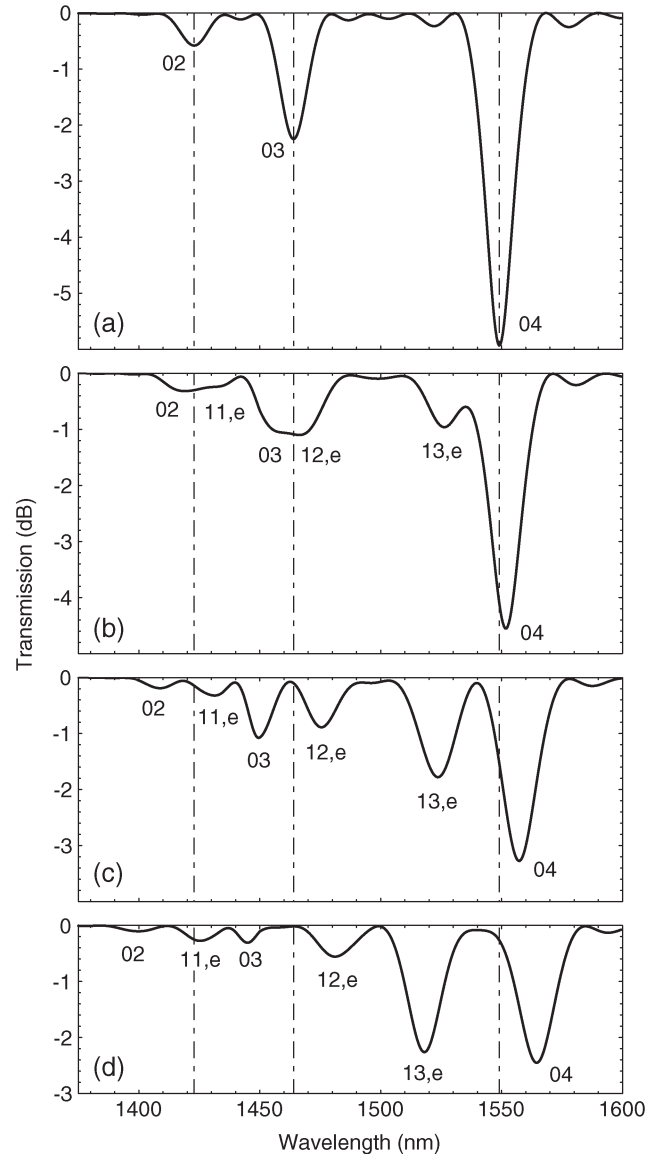

Fig. 6. (a)–(d) Transmission spectra for $\kappa = 0 - 3$ m^{-1}, respectively. Dashed lines indicate phase-matched wavelengths at zero curvature. Notch labels indicate the LP designation of the phase-matched mode at each notch central wavelength. $\Lambda = 560$ μm, $L = 25$ mm.

of attenuation notches shift. Second, new attenuation notches appear and shift in the opposite direction. Finally, the depth of these notches vary with κ.

The wavelength shifts are correlated to the spatial shift of the cladding modes across the fiber cross section. A spatial shift in the $\pm x$-direction results in a change in the mode's phase velocity because it samples an increased or decreased n_{esw}. Contrary to reported behavior for weakly guiding two-layer fibers [21], the cladding modes presented here do not all shift toward $x > 0$ when propagating through a bend. Thus, although most modes travel more slowly in a curved fiber, some will actually propagate with a higher phase velocity. In the set of modes we have numerically analyzed, the first two LP$_{0n}$ cladding modes shift toward the outside of the fiber bend while the third behaves the opposite way. For each of these LP$_{0n}$ modes at $\kappa = 0$, there is a neighboring LP$_{1(n-1)}$ mode whose spatial location, and thus n_{eff}, shift counter to that of the LP$_{0n}$

mode as curvature is applied to an initially straight fiber. This explains why it appeared as if the notches of an LPFG were splitting from a single notch [12]–[14], [16]–[18].

Additionally, the fact that the mode behavior seems to reverse for the higher order cladding modes supports the data published by Liu *et al.* in [14, Fig. 2(a)]. These data show wavelength shifts of the initial LP_{0n} notches reversing direction at longer wavelengths. More extensive analysis detailing modes with higher order radial symmetry as well as using the actual fiber parameters from [14] would be necessary to attempt to accurately model their results.

As a fiber is bent, the LP_{0n} cladding modes shift in the $\pm x$-direction. The overlap of the core mode with these fields, which initially have a local maximum at the fiber center, tends to decrease with applied curvature. Thus, for a grating that is not overcoupled initially, the original attenuation notches shift in wavelength and decrease in depth as curvature is applied. In contrast, the LP_{1n} cladding modes have zero intensity at the center of a straight fiber and are antisymmetric across the fiber axis. As the fiber is bent, the spatial shift of these modes makes them overlap with the core mode, which leads to new LPFG notches. These new notches initially increase in magnitude as curvature is increased, as is shown in Fig. 5, before flattening out at a level similar to each neighboring LP_{0n} notch. This behavior is also in good agreement with published experimental demonstrations [12]–[14].

In summary, we have shown that the interesting spectral behavior of UV-induced LPFGs subject to bending is due to bend-induced changes in the cladding-mode profiles. These changes permit coupling between modes with initially differing azimuthal symmetries even with an induced periodic perturbation that is uniform across the fiber core. Numerical modeling of the modes of a three-layer cylindrical waveguide allowed prediction of the changes in wavelength and attenuation as bending is introduced. These predictions agree well with published transmission spectra from experimental devices. This understanding of the effects in a curved LPFG will be necessary for developing future devices with specific design goals.

REFERENCES

[1] A. M. Vengsarkar, P. J. Lemaire, J. B. Judkins, V. Bhatia, T. Erdogan, and J. E. Sipe, "Long-period fiber gratings as band-rejection filters," *J. Lightw. Technol.*, vol. 14, no. 1, pp. 58–65, Jan. 1996.
[2] T. Erdogan, "Fiber grating spectra," *J. Lightw. Technol.*, vol. 15, no. 8, pp. 1277–1294, Aug. 1997.
[3] ——, "Cladding-mode resonances in short- and long-period fiber grating filters," *J. Opt. Soc. Amer. A, Opt. Image Sci. Vis.*, vol. 14, no. 8, pp. 1760–1773, Aug. 1997.
[4] S. Savin, M. J. F. Digonnet, G. S. Kino, and H. J. Shaw, "Tunable mechanically induced long-period fiber gratings," *Opt. Lett.*, vol. 25, no. 10, pp. 710–712, May 2000.
[5] T.-Y. Tang, P.-Y. Tseng, C.-Y. Chiu, C.-N. Lin, C. C. Yang, Y.-W. Kiang, and K.-J. Ma, "Long-period fiber grating effects induced by double-sided loading," *Opt. Eng.*, vol. 42, no. 7, pp. 1910–1914, Jul. 2003.
[6] H. S. Kim, S. H. Yun, I. K. Kwang, and B. Y. Kim, "All-fiber acousto-optic tunable notch filter with electronically controllable spectral profile," *Opt. Lett.*, vol. 22, no. 19, pp. 1476–1478, Oct. 1997.
[7] A. M. Vengsarkar, J. R. Pedrazzani, J. B. Judkins, P. J. Lemaire, N. S. Bergano, and C. R. Davidson, "Long-period fiber-grating-based gain equalizers," *Opt. Lett.*, vol. 21, no. 5, pp. 336–338, Mar. 1996.
[8] V. Bhatia and A. M. Vengsarkar, "Optical fiber long-period grating sensors," *Opt. Lett.*, vol. 21, no. 9, pp. 692–694, May 1996.
[9] V. Bhatia, "Applications of long-period gratings to single and multi-parameter sensing," *Opt. Express*, vol. 4, no. 11, pp. 457–466, May 1999.
[10] H. J. Patrick, C. C. Chang, and S. T. Vohra, "Long period fibre gratings for structural bend sensing," *Electron. Lett.*, vol. 34, no. 18, pp. 1773–1775, Sep. 1998.
[11] C. C. Ye, S. W. James, and R. P. Tatam, "Simultaneous temperature and bend sensing with long-period fiber gratings," *Opt. Lett.*, vol. 25, no. 14, pp. 1007–1009, Jul. 2000.
[12] Y. Liu, L. Zhang, J. A. R. Williams, and I. Bennion, "Optical bend sensor based on measurement of resonance mode splitting of long-period fiber grating," *IEEE Photon. Technol. Lett.*, vol. 12, no. 5, pp. 531–533, May 2000.
[13] ——, "Bend sensing by measuring the resonance splitting of long-period fiber gratings," *Opt. Commun.*, vol. 193, no. 1/6, pp. 69–72, Jun. 2001.
[14] Y. Liu, M. N. Ng, K. S. Chiang, and J. Yao, "Long-period fiber grating curvature sensor based on temperature-insensitive wavelength separation measurements," in *Proc. Advanced Photonic Sensors and Applications II*, Singapore, Nov. 27–30, 2001, vol. 4596, pp. 104–109.
[15] Z. Chen, K. S. Chiang, M. N. Ng, Y. M. Chan, and H. Ke, "Bent long-period fiber gratings for sensor applications," in *Proc. Advanced Photonic Sensors and Applications*, Singapore, Nov. 30–Dec. 3, 1999, vol. 3897, pp. 94–104.
[16] D. A. Gonzalez, J. L. Arce-Diego, A. Cobo, and J. M. Lopez-Higuera, "Spectral modelling of curved long-period fibre gratings," *Meas. Sci. Technol.*, vol. 12, no. 7, pp. 786–792, Jul. 2001.
[17] S. W. James, C. C. Ye, S. Khaliq, and R. P. Tatam, "Bend sensing using optical fibre long period gratings," in *Proc. 14th Int. Conf. Optical Fiber Sensors (OFS)*, Venice, Italy, Oct. 11–13, 2000, pp. 66–69.
[18] C. C. Ye, C. Wei, S. Khaliq, S. W. James, P. E. Irving, and R. P. Tatam, "Bend sensing in structures using long-period optical fibre gratings," in *Proc. 5th Eur. Conf. Smart Structures and Materials*, Glasgow, U.K., May 22–24, 2000, vol. 4073, pp. 311–315.
[19] J. L. Arce-Diego, D. Pereda-Cubian, and M. A. Muriel, "Polarization effects in short- and long-period fibre gratings: A generalized approach," *J. Opt., A Pure Appl. Opt.*, vol. 6, no. 3, pp. S45–S51, Mar. 2004.
[20] M. Heiblum and J. H. Harris, "Analysis of curved optical waveguides by conformal transformation," *IEEE J. Quantum Electron.*, vol. QE-11, no. 2, pp. 75–83, Feb. 1975.
[21] D. Marcuse, "Field deformation and loss caused by curvature of optical fibers," *J. Opt. Soc. Amer.*, vol. 66, no. 4, pp. 311–320, Apr. 1976.
[22] A. M. Smith, "Birefringence induced by bends and twists in single-mode optical fiber," *Appl. Opt.*, vol. 19, no. 15, pp. 2606–2611, Aug. 1980.
[23] V. Dangui, M. J. F. Digonnet, and G. S. Kino, "A fast and accurate numerical tool to model the mode properties of photonic bandgap fibers," in *Proc. Optical Fiber Communication Conf. (OFC)*, Anaheim, CA, Mar. 6–11, 2005.
[24] *Corning Single-Mode Optical Fiber: Smf-28*. [Online]. Available: http://www.corningfiber.com/
[25] J. W. Fleming, "Dispersion in GeO_2-SiO_2 glasses," *Appl. Opt.*, vol. 23, no. 24, pp. 4486–4493, Dec. 1984.
[26] C. Tsao, *Optical Fibre Waveguide Analysis*. New York: Oxford Univ. Press, 1992.

Ueyn L. Block received the B.S. degree in physics and mathematics from New Mexico Institute of Mining and Technology, Socorro, in 1998, where he performed research in atmospheric physics. He received the M.S. degree in applied physics from Stanford University, Stanford, CA, in 2001 and is currently working toward the Ph.D. degree in applied physics at the same university.

Currently, he is a Research Assistant in the Ginzton Laboratory at Stanford University. His research interests include modeling of fiber gratings, automatic gain equalization in optical fiber amplifiers, and multiwavelength fiber lasers.

Vinayak Dangui received the Diplome d'Ingenieur from Ecole Polytechnique, Paris, France, in 2000, where he performed research in nitride semiconductor lasers. He received the M.S. degree in electrical engineering from Stanford University, Stanford, CA, in 2002 and is currently working toward the Ph.D. degree in electrical engineering at the same university.

Currently, he is a Research Assistant in the Ginzton Laboratory at Stanford University. His research interests include modeling of photonic-bandgap fibers and photonic-bandgap fiber components.

Michel J. F. Digonnet (M'01) received the degree of engineering from Ecole Supérieure de Physique et de Chimie de la Ville de Paris, the Diplome d'Etudes Approfondies in coherent optics from the University of Paris, Orsay, France, in 1978, and the M.S. and Ph.D. degrees from the Applied Physics Department, Stanford University, Stanford, CA, in 1980 and 1983, respectively. His doctoral research centered on wavelength division multiplexing (WDM) fiber couplers and single-crystal fiber lasers and amplifiers.

From 1983 to 1986, he was employed by Litton Guidance and Control, Chatsworth, CA, as a Visiting Scholar at Stanford, conducting research in miniature solid-state sources and integrated optics for fiber sensors. From 1986 to 1990, he was involved in the development of dye and 2-μm solid-state lasers, fiber sensors, and delivery systems for laser angioplasty at MCM Laboratories, Mountain View, CA. Since then, he has been a Senior Research Associate in Stanford University's Applied Physics Department. His current interests include photonic-bandgap fibers, fiber sensors and sensor arrays, high-power ceramic and fiber lasers and amplifiers, fiber gratings, optical microcavities, and poled glasses. He has published 175 articles, issued 55 patents, edited several books, taught courses in fiber amplifiers, lasers, and sensors, and chaired numerous conferences on optical fiber devices and fiber sensors.

Martin M. Fejer (M'03), photograph and biography not available at the time of publication.